Editors' Suggestion | Featured in Physics

Excitation Spectrum of a Trapped Dipolar Supersolid and Its Experimental Evidence

G. Natale,[1] R. M. W. van Bijnen,[2] A. Patscheider,[1] D. Petter,[1] M. J. Mark,[1,2] L. Chomaz,[1] and F. Ferlaino[1,2,*]
[1]Institut für Experimentalphysik, Universität Innsbruck, Technikerstraße 25, 6020 Innsbruck, Austria
[2]Institut für Quantenoptik und Quanteninformation, Österreichische Akademie der Wissenschaften, Technikerstraße 21a, 6020 Innsbruck, Austria

(Received 3 July 2019; published 1 August 2019)

We study the spectrum of elementary excitations of a dipolar Bose gas in a three-dimensional anisotropic trap across the superfluid-supersolid phase transition. Theoretically, we show that, when entering the supersolid phase, two distinct excitation branches appear, respectively associated with dominantly crystal and superfluid excitations. These results confirm infinite-system predictions, showing that finite-size effects play only a small qualitative role, and connect the two branches to the simultaneous occurrence of crystal and superfluid orders. Experimentally, we probe compressional excitations in an Er quantum gas across the phase diagram. While in the Bose-Einstein condensate regime the system exhibits an ordinary quadrupole oscillation, in the supersolid regime we observe a striking two-frequency response of the system, related to the two spontaneously broken symmetries.

DOI: 10.1103/PhysRevLett.123.050402

Supersolidity—a paradoxical quantum phase of matter that combines crystal rigidity and superfluid flow—was suggested more than half a century ago as a paradigmatic manifestation of a state in which two continuous symmetries are simultaneously broken [1]. In a supersolid, the spontaneously broken symmetries are the gauge symmetry, associated with the phase coherence in a superfluid, and the translational invariance, signalizing crystalline order. The striking aspect is that, in a supersolid of indistinguishable bosons, the same particles are participating in developing such two apparently antithetical, yet coexisting, orders. Originally predicted in quantum solids with mobile bosonic vacancies [2–4], the search for supersolidity has fueled research across different areas of quantum matter from condensed matter to atomic physics, including quantum gases with nonlocal interparticle interactions [5–19].

Recent experiments have revealed that axially elongated dipolar quantum gases can undergo a phase transition from a regular Bose-Einstein condensate (BEC), possessing a homogeneous density in the local-density-approximation sense, to a state with supersolid properties, where density modulation and global phase coherence coexist [15–17]. Such experiments, complementing the ones with BECs coupled to light [20–22], have opened a whole set of fundamental questions, covering the very real meaning of superfluidity in a supersolid state, its shear transport, and phase rigidity.

Of particular relevance is the study of the spectrum of elementary excitations, which governs the system response to perturbations [23–25]. Typically, phase transitions occur in concomitance with drastic modifications of the excitation spectra—as in the case of the emergence of roton excitations in He II or the phononic dispersion for BECs—and similar dramatic changes are expected when crossing the superfluid-supersolid transition. Theoretical studies of uniform (infinite) gases with periodic boundary conditions and soft-core [26–28] or dipolar interactions [14,29,30] have shown two distinct branches appearing in the excitation spectrum of a supersolid state—one for each broken symmetry. Their coexistence has been identified as an unambiguous proof of supersolidity, being the direct consequence of the simultaneous presence of superfluid and crystalline orders [2,26,27,31].

An important issue is to understand if these trademarks survive—and can be measured—in the experimentally relevant regimes of a finite-size quantum gas, confined in all three spatial dimensions. In this Letter, we address these points by performing full spectrum calculations and by experimentally exciting collective modes in an erbium quantum gas. Both the theory and experiment show the existence of two distinct classes of excitations, one connected to crystal modes and the other to phase modes, providing the finite-size equivalent of the two-branches spectrum for infinite systems.

In our study, we consider a three-dimensional dipolar quantum gas confined in an axially elongated (y) harmonic trap with transverse orientation (z) of the atomic dipoles. These systems are well described by an extended Gross-Pitaevskii equation (EGPE), including nonlinear terms, accounting for contact interactions depending on the scattering length a_s, the anisotropic long-range dipole-dipole interaction (DDI), and quantum fluctuations in the form of a Lee-Huang-Yang type of correction [12,14–17,19,32–36]; see also Ref. [37]. We calculate ground-state wave functions $\psi_0(\mathbf{r})$ by minimizing the energy functional resulting from the EGPE using the conjugate-gradients technique [46].

 © 2019 American Physical Society

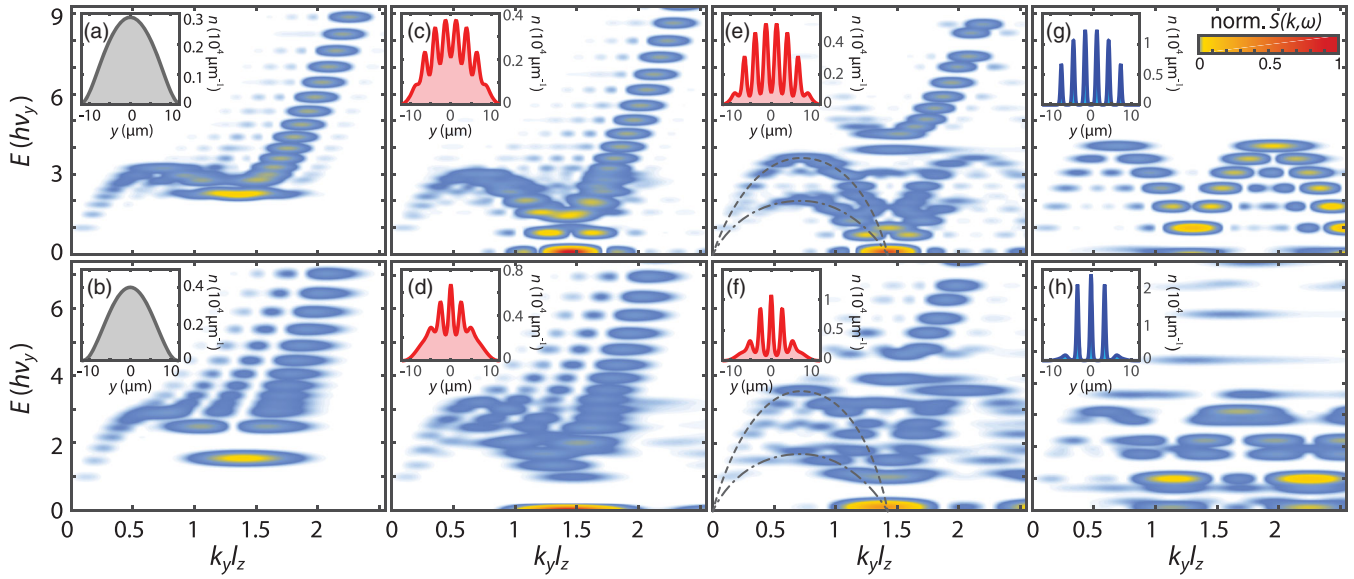

FIG. 1. Axial excitation spectra of a trapped dipolar quantum gas across the BEC-supersolid-ID phase transition. The trap frequencies are $2\pi \times (260, 29.6, 171)$ Hz. The upper (lower) row shows calculations for a ^{164}Dy (^{166}Er) quantum gas of 4×10^4 (5×10^4) atoms in the BEC (a),(b), supersolid (c)–(f), and ID (g),(h) regimes, together with the corresponding ground-state density profiles (insets). (a), (c), (e), and (g) correspond to $a_s = (92, 91, 90, 81)a_0$, and (b), (d), (f), and (h) to $a_s = (50.8, 50.5, 50, 48)a_0$, respectively. In (e) and (f), the dashed and dash-dotted lines are guides to the eyes, indicating the two excitation branches. The color map indicates the calculated DSF, and l_z is the harmonic oscillator length along the dipoles' direction.

As shown in Fig. 1 (insets), the ground state evolves with decreasing a_s from a regular BEC (a), (b) to a supersolid state with axial density-wave modulation (c)–(f) and finally to an insulating array of independent droplets (ID) (g), (h) [7,14,15,17,27].

The spectrum of elementary excitations is calculated by numerically solving the Bogoliubov–de Gennes equations, which are obtained from an expansion of the macroscopic wave function as $\psi(\mathbf{r},t) = [\psi_0(\mathbf{r}) + \eta(u_l e^{-i\epsilon_l t/\hbar} + v_l^* e^{i\epsilon_l t/\hbar})]e^{-i\mu t}$ with $\eta \ll 1$ and linearizing the EGPE around ψ_0 [13,25,46,47]. Here, μ is the ground state's chemical potential. By solving the resulting eigenvalue problem, we find a set of discrete modes, numbered by l, of energy $\epsilon_l = \hbar\omega_l$ and amplitudes u_l and v_l. We calculate the dynamic structure factor (DSF) $S(k,\omega)$, which informs on the system's response when its density is perturbed at a given modulation momentum k and with an energy $\hbar\omega$ [25,48,49]. Whereas in the absence of an external trap the spectrum is continuous and the DSF is a δ-peak resonance at the Bogoliubov mode (ω_l, k_l), the confining potential yields instead a discretization of the excitation spectrum and a k broadening in $S(k,\omega)$. For a given energy (i.e., a single mode), finite-size effects may even yield several peaks in k; see, e.g., three-peak structures at large energy in Figs. 1(a) and 1(b). For the considered parameters, these finite-size effects are more pronounced in Er than Dy, since the latter exhibits a larger number of maxima in the density-modulated phases, rendering its excitation spectrum more reminiscent of the infinite-system case; see Fig. 1.

Figure 1 shows the calculated excitation spectrum for ground states in the regular BEC, the supersolid, and the ID phases for a Dy (upper row) and Er (lower row) quantum gas. In the BEC regime close to the supersolid transition [Figs. 1(a) and 1(b)], the spectrum of excitations shows a single excitation branch with the characteristic phonon-maxon-roton dispersion of a BEC [50–54], as recently measured [55]. When the roton fully softens (at $a_s = a_s^*$), the ground state becomes density modulated with a wave number close to the roton one, k_{rot}. Here, the excitation spectrum develops additional structures, marked by the appearance of nearly degenerate modes [Figs. 1(c) and 1(d)]. When lowering a_s, we find that these modes start to separate in energy, where some harden and the others soften, and two excitation branches become visible [Figs. 1(e) and 1(f)]. This result resembles that of infinite systems, where the broken translational and gauge symmetry are each associated with the appearance of one excitation branch [14,26,27]. Additionally, we observe that the spectrum acquires a periodic structure, reminiscent of Brillouin zones in a crystal, with reciprocal lattice constant $k \simeq k_{\mathrm{rot}}$. Modes with an energy higher than the maxon (energy maximum at $k < k_{\mathrm{rot}}$) seem to have a single-droplet-excitation character, and they will be the subject of future investigations. When further decreasing $a_s < a_s^*$, the lower-lying branch decreases both in energy and in DSF values, whereas the opposite occurs for the higher branch. Eventually, when reaching the ID regime, the lower branch progressively vanishes, underlying the disappearance of global superfluidity [Figs. 1(g) and 1(h)].

We focus on the properties of the excitation spectrum in the supersolid regime. The interesting question is how the two branches relate to the two orders in the systems, crystal and superfluid. To gain insight, we study the system's dynamics when a single mode l is excited with amplitude $\eta \ll 1$ by writing $\psi(t)e^{i\mu t} \approx \sqrt{|\psi_0|^2 + 2\eta\delta\rho_l \cos\omega_l t}e^{-i\eta\delta\varphi_l \sin\omega_l t}$, in terms of density perturbations $\delta\rho_l = (u_l + v_l^*)|\psi_0|$ and phase perturbations $\delta\varphi_l = (u_l - v_l^*)/|\psi_0|$. The subsequent time evolution of the axial density profile is shown in Figs. 2(a)–2(c) for three relevant cases. For simplicity, only the two extremes of the mode oscillation are shown. The mode character can be understood by noting that phase gradients correspond to mass currents. Large gradients *inside* a density peak imply motion of the density peak [e.g., Fig. 2(a)] and relate to *crystal modes*. Large phase gradients *between* density peaks signify a superfluid current of particles tunneling from one density peak to another [e.g., Fig. 2(b)] and are associated with *phase modes*. However, in our system, the phase or crystal mode classification is not strict, and we find that these two characters mix; see Figs. 2(a)–2(c). Particularly, we observe both behaviors simultaneously in Fig. 2(c). Such a mixing is expected from the long-range nature of the DDI, coupling density, and position of the peaks [26,27]. Note that the character of the mode can change with a_s. For instance, the mode in Fig. 2(c) develops an almost pure crystal character for decreasing a_s. To quantify a mode's character, we plot in Fig. 2(d) the DSF spectrum at a fixed a_s, colored

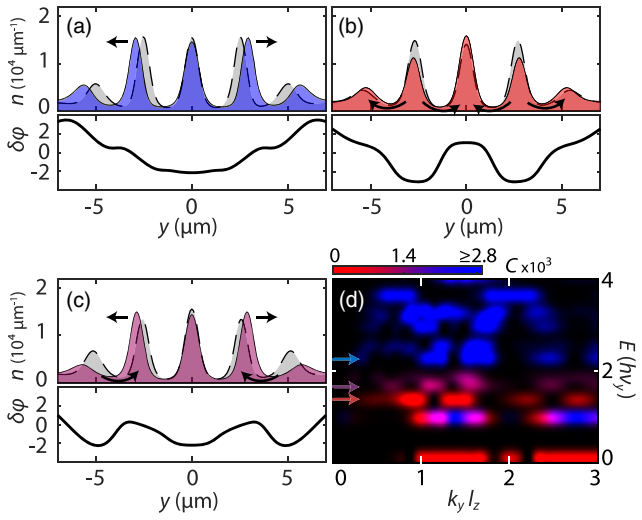

FIG. 2. Evolution of three different even modes of the system calculated for 5×10^4 Er atoms at $a_s = 49.8a_0$: (a) fourth-, (b) second-, and (c) third-lowest-lying even modes in energy with frequencies (67.4, 40.3, 49.8) Hz, corresponding to crystal, phase, and mixed modes, respectively. Each panel shows $n = |\psi(0, y, 0, t)|^2$ for $t = \pi/2\omega_l$ and $t = 3\pi/2\omega_l$ with $\eta = 0.15$ and the corresponding $\delta\varphi(0, y, 0)$. (d) DSF for the same setting as in (a)–(c), where the modes are colored according to their associated phase (red) or crystal (blue) character via C [37].

according to the ratio C of phase variances inside, and between the density peaks [37]. This allows us to differentiate the dominant character of the two branches, being phase type for the lower branch and crystal type for the upper one.

To test our predictions, we experimentally study the collective excitations in an erbium quantum gas across the BEC-supersolid-ID phases. We prepare a BEC at $a_s = 64a_0$. The atoms are confined in an axially elongated optical-dipole trap of harmonic frequencies $2\pi \times (\nu_x, \nu_y, \nu_z) = 2\pi \times (259(2), 30(1), 170(1))$ Hz and polarized along z by an external magnetic field; see Refs. [13,17]. To probe our system, we perform standard absorption imaging after 30 ms of time-of-flight expansion, yielding measurements of the momentum space density $n(k_x, k_y)$ [37]. Using the tunability of the contact interaction via magnetic Feshbach resonances [56], we can prepare the system at desired locations in the phase diagram in the BEC, supersolid, or ID phase by linearly ramping down a_s in 20 ms to the target value. We then allow the system to stabilize for 10 ms. At this point, we record an atom number of typically 5×10^4 for the supersolid regime. We confirmed the relevant a_s ranges by repeating the matter-wave interferometric analysis of Ref. [17]. While in the BEC region the momentum distribution shows a regular, nearly Gaussian single peak, in the supersolid regime the in-trap density modulation gives rise to coherent interference patterns along k_y, consisting of a central peak with two lower-amplitude side peaks; see Fig. 3(a).

After preparing the system in the desired phase, we excite collective modes in the gas by suddenly reducing the axial harmonic confinement to 10% of its initial value (i.e., $\nu_y \approx 3$ Hz) for 1 ms, before restoring it again. The atomic cloud is subsequently held for a variable time t_h, before releasing it from the trap and recording the time evolution of $n(k_x, k_y)$. As the lifetime of the supersolid state is limited to around 40 ms [17], we focus on $t_h \leq 30$ ms. As expected, in the BEC phase, we predominantly observe an oscillation of the axial width, connected to the lowest-lying quadrupole mode [25]. In the supersolid regime, the situation is more complex; see Figs. 1(c)–1(f). Here, multiple modes, of both crystal and phase character, can be simultaneously populated, resulting in a convoluted dynamics of the interference pattern.

We therefore employ a *model-free* statistical approach, known as principal component analysis (PCA) [57], to study the time evolution of the measured interference patterns at a fixed a_s. This method has been successfully used to study e.g., matter-wave interference [58] and collective excitations [59] in ultracold-gas experiments. The PCA analyzes the correlations between pixels in a set of images, decomposes them into statistically independent components, and orders these principal components (PCs) according to their contributions to the overall fluctuations in the dataset.

In a dataset probing the system dynamics after an excitation, the PCA can identify the elementary modes

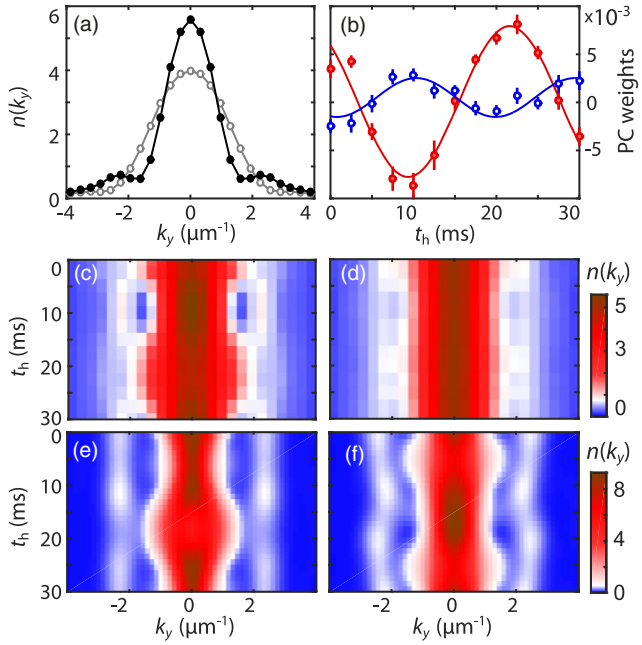

FIG. 3. (a) Example of a measured mean interference pattern in the renormalized central cut of the density distribution $n(k_y)$ for $t_h = 5$ ms in the supersolid regime at $a_s = 49.8a_0$ (filled circles) and in the BEC regime at $a_s = 51.7a_0$ (open circles). (b)–(d) PCA results at $a_s = 49.8a_0$. (b) Time evolution of the weights of PC1 (filled circles) and PC2 (open circles) together with their sine fit. Error bars denote the standard error of the mean. (c),(d) Evolution of the partially recomposed $n(k_y)$ accounting for the population of PC1 (c) and PC2 (d) only. (e),(f) Calculated time evolution of $n(k_y)$ from excitation of the mode shown in Figs. 2(b) and 2(c), respectively, and using $\eta = 0.15$.

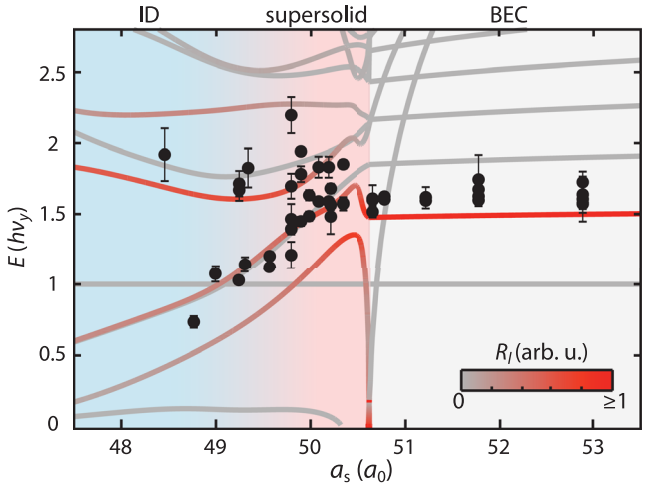

FIG. 4. Comparison between the mode energy obtained from the theory calculations and the energies extracted from the PCs (circles). The gradual color code of the theory lines represents the relative strength of R_l going from strong (red) to no (gray) coupling. Error bars denote one standard deviation from the fit. The background color indicates the BEC, supersolid, and ID regions (see upper labels), identified using a matter-wave interferometric analysis of the experimental data [17].

with the PC weights in the individual images exhibiting oscillations at the mode frequencies [37,59]. We apply the PCA to the time evolution of the interference patterns after the trap excitation. Figure 3(b) shows the PCA results in the supersolid regime at $a_s = 49.8a_0$. We identify two leading PCs, which we label as PC1 and PC2. Their weights oscillate with different amplitudes and at distinct frequencies, namely, 41(1) Hz for PC1 and 52(5) Hz for PC2. The comparison between the measured frequencies and the theoretically calculated mode energies indicates that, following our trap excitation, the second- and third-lowest-lying even modes are simultaneously populated. As shown in Figs. 2(b) and 2(c), these modes possess a phase and a mixed character, respectively. Note that we apply an overall shift of $-4.3a_0$ to the a_s value for the experimental data; for more details, see the discussion in Refs. [55,60].

To visualize the role of each PC on the interference-pattern dynamics, we apply a partial recomposition of the images, accounting only for the PC of interest; see Ref. [37]. The effect of PC1 on the axial dynamics is shown in Fig. 3(c), mainly being an axial breathing of the central peak, accompanied by weaker in-phase breathing of the side peaks. Instead, PC2 exhibits a dominant variation of the side-peak amplitude; see Fig. 3(d). These results show a good agreement with the calculated time evolutions of the interference patterns for the second and third even modes, shown in Figs. 3(e) and 3(f).

Finally, we study the evolution of the modes across the BEC to supersolid and ID phases. We repeat the collective excitation measurements for various a_s, and, using the PCA, we extract the oscillation frequencies of all the leading PCs. Figure 4 shows our experimental results together with the mode tracking from the spectrum calculations. For a give elementary mode l, we plot ω_l as well as the response amplitude $R_l = m\omega_y^2\langle\ell|\hat{y}^2|0\rangle/2\hbar\omega_l$, which indicates the probability to be excited by our trap-excitation scheme. For completeness, the figure shows both even and odd modes, although only even modes are coupled to our trap-excitation scheme. Here, $|0\rangle$ and $|\ell\rangle$ denote, respectively, the ground and excited states of interest, and $\hat{y}$ is the axial position operator.

In the BEC regime, besides the roton mode that progressively softens with decreasing a_s, the other modes show a regular spacing in energy and are nearly constant with a_s. In both the theory and experiment, we observe that just one mode couples to the trap-excitation scheme. This mode has a compressional, axial breathing character. Experimentally, we observe that all the leading PCs oscillate at the same frequency, suggesting that they account for the same mode [37]. In this regime, both the PC frequencies ω_l and R_l remain rather constant. At the supersolid phase transition, reached around $a_s = 50.6a_0$, the numerical calculations reveal that different modes undergo an abrupt change and can mix with each other.

Their energy and phase or crystal character exhibits a strong dependence on a_s. Here, several modes respond to the trap-excitation scheme, as shown by the value of R_l. In the PCA, we observe that the leading PCs now oscillate at distinct frequencies and have different characters (see also Fig. 3). One set of PCs reduces their frequency when lowering a_s, indicating (at least) one phase mode that softens strongly in the supersolid regime, even below the trap frequency ν_y. Another set of PCs shows a frequency that remains hard when decreasing a_s. Calculations of C show that this mode changes character along the phase diagram and eventually becomes crystal type.

In conclusion, the overall agreement between the experiment and theory confirms the calculations in the supersolid regime, revealing two distinct branches with respective crystal and superfluid characters. The trademarks of supersolidity expected in infinite systems thus carry over to the finite-size ones currently available in laboratories. The knowledge of the excitation spectrum will provide the base for future investigations related to the superfluid properties and phase rigidity in a supersolid state.

We thank D. Baillie, R. Bisset, B. Blakie, T. Pfau, A. Recati, L. Santos, and P. Silvi for stimulating discussions. We acknowledge useful conversations with the participants of the meeting on "Perspectives for supersolidity in dipolar droplet arrays" in Stuttgart, where we became aware of related work by the groups of Modugno [61] and Pfau [62]. Part of the computational results presented have been achieved using the HPC infrastructure LEO of the University of Innsbruck. This work is financially supported through an ERC Consolidator Grant (RARE, no. 681432) and a DFG/FWF (FOR 2247/PI2790), and the project PASQUANS of the EU Quantum Technology flagship.

*To whom all correspondence should be addressed.
Francesca.Ferlaino@uibk.ac.at

[1] M. Boninsegni and N. V. Prokof'ev, Rev. Mod. Phys. **84**, 759 (2012).
[2] A. F. Andreev and I. M. Lifshitz, Sov. Phys. JETP **29**, 1107 (1969).
[3] G. V. Chester, Phys. Rev. A **2**, 256 (1970).
[4] A. J. Leggett, Phys. Rev. Lett. **25**, 1543 (1970).
[5] N. Henkel, R. Nath, and T. Pohl, Phys. Rev. Lett. **104**, 195302 (2010).
[6] F. Cinti, P. Jain, M. Boninsegni, A. Micheli, P. Zoller, and G. Pupillo, Phys. Rev. Lett. **105**, 135301 (2010).
[7] M. Boninsegni, J. Low Temp. Phys. **168**, 137 (2012).
[8] Z.-K. Lu, Y. Li, D. S. Petrov, and G. V. Shlyapnikov, Phys. Rev. Lett. **115**, 075303 (2015).
[9] A. Macia, J. Sánchez-Baena, J. Boronat, and F. Mazzanti, Phys. Rev. Lett. **117**, 205301 (2016).
[10] F. Cinti and M. Boninsegni, Phys. Rev. A **96**, 013627 (2017).
[11] M. Wenzel, F. Böttcher, T. Langen, I. Ferrier-Barbut, and T. Pfau, Phys. Rev. A **96**, 053630 (2017).
[12] D. Baillie and P. B. Blakie, Phys. Rev. Lett. **121**, 195301 (2018).
[13] L. Chomaz, R. M. W. van Bijnen, D. Petter, G. Faraoni, S. Baier, J. H. Becher, M. J. Mark, F. Wächtler, L. Santos, and F. Ferlaino, Nat. Phys. **14**, 442 (2018).
[14] S. M. Roccuzzo and F. Ancilotto, Phys. Rev. A **99**, 041601 (R) (2019).
[15] F. Böttcher, J.-N. Schmidt, M. Wenzel, J. Hertkorn, M. Guo, T. Langen, and T. Pfau, Phys. Rev. X **9**, 011051 (2019).
[16] L. Tanzi, E. Lucioni, F. Famà, J. Catani, A. Fioretti, C. Gabbanini, R. N. Bisset, L. Santos, and G. Modugno, Phys. Rev. Lett. **122**, 130405 (2019).
[17] L. Chomaz, D. Petter, P. Ilzhöfer, G. Natale, A. Trautmann, C. Politi, G. Durastante, R. M. W. van Bijnen, A. Patscheider, M. Sohmen, M. J. Mark, and F. Ferlaino, Phys. Rev. X **9**, 021012 (2019).
[18] Y. Kora and M. Boninsegni, arXiv:1902.08256.
[19] Y.-C. Zhang, F. Maucher, and T. Pohl, Phys. Rev. Lett. **123**, 015301 (2019).
[20] J. Léonard, A. Morales, P. Zupancic, T. Esslinger, and T. Donner, Nature (London) **543**, 87 (2017).
[21] J.-R. Li, J. Lee, W. Huang, S. Burchesky, B. Shteynas, F. Ç. Top, A. O. Jamison, and W. Ketterle, Nature (London) **543**, 91 (2017).
[22] J. Léonard, A. Morales, P. Zupancic, T. Donner, and T. Esslinger, Science **358**, 1415 (2017).
[23] L. D. Landau, J. Phys. (Moscow) **11**, 91 (1947).
[24] N. N. Bogoliubov, J. Phys. USSR **11**, 23 (1947).
[25] L. Pitaevskii and S. Stringari, *Bose-Einstein Condensation and Superfluidity* (Oxford University Press, Oxford, 2016), Vol. 164.
[26] S. Saccani, S. Moroni, and M. Boninsegni, Phys. Rev. Lett. **108**, 175301 (2012).
[27] T. Macrì, F. Maucher, F. Cinti, and T. Pohl, Phys. Rev. A **87**, 061602(R) (2013).
[28] S. Rossotti, M. Teruzzi, D. Pini, D. E. Galli, and G. Bertaina, Phys. Rev. Lett. **119**, 215301 (2017).
[29] A. Macia, D. Hufnagl, F. Mazzanti, J. Boronat, and R. E. Zillich, Phys. Rev. Lett. **109**, 235307 (2012).
[30] R. Bombin, J. Boronat, and F. Mazzanti, Phys. Rev. Lett. **119**, 250402 (2017).
[31] Y. Pomeau and S. Rica, Phys. Rev. Lett. **72**, 2426 (1994).
[32] F. Wächtler and L. Santos, Phys. Rev. A **93**, 061603(R) (2016).
[33] R. N. Bisset, R. M. Wilson, D. Baillie, and P. B. Blakie, Phys. Rev. A **94**, 033619 (2016).
[34] F. Wächtler and L. Santos, Phys. Rev. A **94**, 043618 (2016).
[35] M. Schmitt, M. Wenzel, F. Böttcher, I. Ferrier-Barbut, and T. Pfau, Nature (London) **539**, 259 (2016).
[36] L. Chomaz, S. Baier, D. Petter, M. J. Mark, F. Wächtler, L. Santos, and F. Ferlaino, Phys. Rev. X **6**, 041039 (2016).
[37] Supplemental Material at http://link.aps.org/supplemental/10.1103/PhysRevLett.123.050402, which includes Refs. [38–45] and details on the analysis and theory calculations.
[38] I. Ferrier-Barbut, M. Wenzel, F. Böttcher, T. Langen, M. Isoard, S. Stringari, and T. Pfau, Phys. Rev. Lett. **120**, 160402 (2018).
[39] C. R. Cabrera, L. Tanzi, J. Sanz, B. Naylor, P. Thomas, P. Cheiney, and L. Tarruell, Science **359**, 301 (2018).

[40] A. Gammal, T. Frederico, L. Tomio, and P. Chomaz, J. Phys. B **33**, 4053 (2000).
[41] A. Bulgac, Phys. Rev. Lett. **89**, 050402 (2002).
[42] A. R. P. Lima and A. Pelster, Phys. Rev. A **84**, 041604(R) (2011).
[43] T. D. Lee and C. N. Yang, Phys. Rev. **105**, 1119 (1957).
[44] M. Baranov, Phys. Rep. **464**, 71 (2008).
[45] D. S. Petrov, Phys. Rev. Lett. **115**, 155302 (2015).
[46] S. Ronen, D. C. E. Bortolotti, and J. L. Bohn, Phys. Rev. A **74**, 013623 (2006).
[47] R. M. W. van Bijnen, N. G. Parker, S. J. J. M. F. Kokkelmans, A. M. Martin, and D. H. J. O'Dell, Phys. Rev. A **82**, 033612 (2010).
[48] P. B. Blakie, R. J. Ballagh, and C. W. Gardiner, Phys. Rev. A **65**, 033602 (2002).
[49] A. Brunello, F. Dalfovo, L. Pitaevskii, S. Stringari, and F. Zambelli, Phys. Rev. A **64**, 063614 (2001).
[50] D. H. J. O'Dell, S. Giovanazzi, and G. Kurizki, Phys. Rev. Lett. **90**, 110402 (2003).
[51] L. Santos, G. V. Shlyapnikov, and M. Lewenstein, Phys. Rev. Lett. **90**, 250403 (2003).
[52] P. B. Blakie, D. Baillie, and R. N. Bisset, Phys. Rev. A **86**, 021604(R) (2012).
[53] R. N. Bisset, D. Baillie, and P. B. Blakie, Phys. Rev. A **88**, 043606 (2013).
[54] M. Jona-Lasinio, K. Łakomy, and L. Santos, Phys. Rev. A **88**, 013619 (2013).
[55] D. Petter, G. Natale, R. M. W. van Bijnen, A. Patscheider, M. J. Mark, L. Chomaz, and F. Ferlaino, Phys. Rev. Lett. **122**, 183401 (2019).
[56] C. Chin, R. Grimm, P. S. Julienne, and E. Tiesinga, Rev. Mod. Phys. **82**, 1225 (2010).
[57] I. Jolliffe, *Generalizations and Adaptations of Principal Component Analysis* (Springer, New York, 2002), pp. 373–405.
[58] S. R. Segal, Q. Diot, E. A. Cornell, A. A. Zozulya, and D. Z. Anderson, Phys. Rev. A **81**, 053601 (2010).
[59] R. Dubessy, C. D. Rossi, T. Badr, L. Longchambon, and H. Perrin, New J. Phys. **16**, 122001 (2014).
[60] F. Böttcher, M. Wenzel, J.-N. Schmidt, M. Guo, T. Langen, I. Ferrier-Barbut, T. Pfau, R. Bombín, J. Sánchez-Baena, J. Boronat, and F. Mazzanti, arXiv:1904.10349.
[61] L. Tanzi, S. Roccuzzo, E. Lucioni, F. Famà, A. Fioretti, C. Gabbanini, G. Modugno, A. Recati, and S. Stringari, arXiv:1906.02791.
[62] M. Guo, F. Böttcher, J. Hertkorn, J.-N. Schmidt, M. Wenzel, H. P. Büchler, T. Langen, and T. Pfau, arXiv:1906.04633.